Acta Biomaterialia 221 (2026) 229–241

Contents lists available at ScienceDirect

Acta Biomaterialia

journal homepage: www.elsevier.com/locate/actbio

Full length article

Time-dependent deformation of the vagina during gestation under controlled pressure

Justin Dubik [a], Aileen Suarez [a], David Dillard [b], Pamela Moalli [c], Raffaella De Vita [a,*]

[a] STRETCH Lab, Department of Mechanical Engineering, Virginia Tech, 330A Kelly Hall, 325 Stanger Street, Blacksburg, 24061, VA, USA
[b] Department of Mechanical Engineering, Virginia Tech, 219A Norris Hall, 495 Old Turner Street, Blacksburg, 24061, VA, USA
[c] Department of Obstetrics, Gynecology, and Reproductive Sciences, University of Pittsburgh School of Medicine; UPMC Magee-Womens Hospital, 300 Halket St, Suite 5600, Pittsburgh, 15213, PA, USA

ARTICLE INFO

Keywords:
Pregnancy-induced remodeling
Vaginal biomechanics
Creep behavior
Inflation testing
Digital image correlation
Collagen microstructure

ABSTRACT

The vagina undergoes extraordinary structural and biomechanical changes throughout pregnancy to facilitate delivery. To characterize the magnitude and temporal progression of these changes, this experimental study quantified the inflation-induced creep response of the murine vagina at multiple gestational time points. Vaginas from non-pregnant (NP), mid-pregnant (MP), and late-pregnant (LP) mice were subjected to two creep tests at luminal pressures of 7 and 14 kPa using a custom free-extension inflation apparatus. Resulting deformations in the longitudinal and circumferential directions were quantified using digital image correlation. Collagen microstructure in NP, MP, and LP vaginas was further examined using second harmonic generation imaging. The MP vagina was significantly stiffer than the NP and LP vagina, suggesting that the organ may stiffen through early-mid pregnancy and then regain compliance toward late pregnancy. Gestation-dependent differences in creep behavior were observed, with the LP vagina exhibiting greater creep than the MP vagina at 7 kPa and more than the NP vagina at 14 kPa. These mechanical adaptations were consistent with gestation-dependent changes in collagen microstructure, including transient fiber reorientation and increased dispersion in MP tissue, followed by partial recovery in LP tissue. The data shed new light on how the vagina remodels in preparation for delivery, and may contribute to future discoveries and developments for improved maternal care.

Statement of Significance:

This study characterizes the time-dependent mechanical behavior of the vagina during pregnancy in a murine model. Using inflation-based biaxial loading and digital image correlation, we quantify deformation during incremental pressurization to prescribed levels and over time at constant pressure. The vagina exhibits reduced compliance at mid-pregnancy and greater time-dependent deformation under sustained loading (creep) in late pregnancy. These changes are associated with collagen remodeling, including alterations in fiber organization, as assessed by second harmonic generation imaging. This behavior corresponds to a transition from a mechanically supportive state that may help maintain pregnancy to a more compliant response that accommodates parturition and reduces the risk of injury. These findings define how the vagina adapts during pregnancy and provide a basis for predictive models of tissue behavior that may help identify abnormal remodeling and improve maternal health outcomes.

1. Introduction

Pregnancy and childbirth impose profound lifelong effects on maternal pelvic health. Extensive remodeling of the vagina and surrounding tissues that occurs before and after vaginal birth can lead to consequences that persist long after delivery [1]. Among the approximately 3.6 million women who give birth annually in the United States [2], the lifetime risk of developing at least one pelvic floor disorder nearly doubles from 11.5% in nulliparous women to 21.1% following childbirth [3], and rises to 30.4% among the two-thirds of women who undergo vaginal delivery [4]. This elevated risk is driven in part by permanent injury associated with maternal birth trauma, which most commonly involves the vagina, with 80% of women undergoing vaginal birth experiencing lacerations [5–7].

The vagina comprises four distinct layers, each characterized by a unique microstructural composition and biological function. Of these,

* Corresponding author.
E-mail address: devita@vt.edu (R. De Vita).

https://doi.org/10.1016/j.actbio.2026.07.025
Received 30 March 2026; Accepted 14 July 2026
Available online 20 July 2026
1742-7061/© 2026 Acta Materialia Inc. Published by Elsevier Inc. All rights are reserved, including those for text and data mining, AI training, and similar technologies.

the muscularis, lamina propria, and adventitia contribute to the tissue's mechanical behavior. The muscularis consists predominantly of smooth muscle and mediates the tissue's active contractile response. The lamina propria, composed of dense connective tissue, and the adventitia, a connective tissue layer that interfaces with and separates surrounding pelvic organs, are rich in fibrillar extracellular matrix components, with collagen serving as the primary load-bearing constituent and elastin present in lower amounts. As a result, alterations in collagen organization across these layers are expected to influence passive mechanical behavior [8]. Variations in the content and organization of these microstructural constituents have been shown to correlate with changes in the mechanical behavior of the vagina [9,10].

The vagina undergoes substantial geometric and structural remodeling during pregnancy to reduce injury and enable vaginal birth. Although gestational changes to the vagina and pelvic floor have been characterized in women [11,12], animal models are more commonly employed to overcome the practical and ethical limitations of human testing. Vaginas from several commonly used laboratory animals share morphological and mechanical features with the human vagina [10, 13], justifying their use as relevant preclinical models. Within these models, pregnancy-associated adaptations of the vagina have been documented at both the geometric and microstructural levels. Using magnetic resonance imaging, our lab has quantified dimensional changes in the murine reproductive tract throughout gestation, revealing increases in vaginal length, diameter, and overall volume as pregnancy progresses toward term [14]. Histological studies have demonstrated microstructural remodeling during pregnancy, including increases in muscularis thickness and smooth muscle content in ewes [15,16]. Pregnancy has also been associated with relative increases in elastin content and decreases in collagen content in ewes [16], with similar changes in collagen content reported in rats [17]. Collectively, these findings indicate that pregnancy induces coordinated geometric and microstructural adaptations of the vagina across species.

Some mechanical adaptations of the vagina during pregnancy have been characterized in preclinical models using a range of *ex vivo* and *in vivo* techniques. Across both murine and ovine models, these studies consistently demonstrate a reduction in vaginal stiffness from the non-pregnant to the late-pregnant state. Using quasi-static uniaxial tensile testing, Ulrich et al. and Rynkevic et al. reported decreases in elastic modulus and strength, along with increased distensibility, in different regions of the sheep vaginal wall loaded in the longitudinal direction (LD) [15,16]. Similar behavior has been observed in the rat vagina, where late-pregnant tissue withstood greater distension and reached lower peak stresses than non-pregnant tissue under incremental distension in the circumferential direction (CD) [18,19]. Complementary *in vivo* studies by Alperin et al. using balloon catheterization further demonstrated that the late-pregnant rat vagina undergoes substantially greater volumetric expansion than the non-pregnant vagina without reaching comparable intravaginal pressures during inflation [20]. Pregnancy is thus associated with a pronounced increase in vaginal compliance across species and loading conditions.

Due to the large loads and deformations experienced by the vagina over time during pregnancy and delivery [21–23], time-dependent mechanical behaviors, such as stress relaxation and creep, are likely to influence its response during delivery. Viscoelastic properties of the vagina have been characterized primarily in non-pregnant tissue. Peña et al. reported that vaginal specimens collected from women with pelvic organ prolapse exhibited approximately 50% reductions in stress within 15 min when held under fixed uniaxial tension in the LD [24]. Using planar biaxial testing, Pack et al. subsequently observed stress relaxation in swine vaginal specimens, with greater relaxation occurring in the LD compared to the CD [25]. More recent investigations have examined vaginal viscoelasticity in murine tissue using inflation-based creep protocols. Clark-Patterson et al. measured changes in vaginal diameter in mice held at fixed axial length and, when recovery was permitted between creep tests, observed increased creep with higher applied pressures [26]. Using free-extension inflation without recovery, our lab characterized the biaxial creep response of rat vaginas under consecutively increasing pressures, observing greater creep in the CD than the LD and diminishing strain increments across successive creep tests [27]. Additional studies have examined vaginal viscoelasticity in the active state, in which smooth muscle contraction was induced via chemical or electrical stimulation [28,29]. Overall, the literature indicates that the vagina exhibits strong direction- and loading-history-dependent viscoelastic behavior; however, its evolution across gestation remains largely unknown, as existing studies primarily compare non-pregnant and late-pregnant tissue, leaving intermediate stages unresolved.

To our knowledge, only one study has investigated pregnancy-related changes in vaginal viscoelasticity [30]. Weli et al. examined creep behavior in non-pregnant and pregnant vaginas, reporting significantly greater deformation in pregnant tissue compared to non-pregnant tissue after 24 h under indentation loading [30]. However, this study was limited to a comparison between non-pregnant and pregnant states and did not resolve how viscoelastic behavior evolves across gestation. A small number of studies have characterized vaginal mechanics at multiple gestational time points, but these have focused on quasi-static behavior. Using uniaxial tensile testing in the LD, Feola et al. reported progressive reductions in elastic modulus and strength with advancing pregnancy in rat vaginas [31]. Lowder et al. performed *en bloc* testing of the rat vagina together with the pelvic floor supportive complex and observed that both mid-pregnant and late-pregnant tissues exhibited reduced stiffness and lower ultimate loads compared to non-pregnant tissue; however, these changes were not progressive, as mid- and late-pregnant responses were similar [32]. More recently, *ex vivo* inflation testing of the intact murine reproductive tract demonstrated coordinated pregnancy-induced mechanical adaptations across the vagina, uterine body, and uterine horns, including increased distensibility in late pregnancy and region-specific deformation patterns [33]. However, the time-dependent mechanical behavior of the vagina itself throughout gestation remains unknown.

In this study, we present the first characterization of vaginal viscoelasticity at distinct gestational stages in a murine model. Mechanical loads were applied via inflation, and local deformations in the LD and CD were quantified using digital image correlation (DIC). Vaginal samples were collected from non-pregnant, mid-pregnant, and late-pregnant mice and subjected to two creep tests at distinct constant pressures, with recovery periods incorporated between tests to minimize the influence of prior loading history [27]. Collagen microstructure was examined at corresponding gestational stages using second harmonic generation (SHG) imaging. These measurements enable evaluation of time-dependent mechanical behavior across gestation and its relationship to collagen microstructure. Overall, this work advances understanding of vaginal remodeling in preparation for delivery and may inform future strategies for improving maternal care.

2. Materials and methods

2.1. Specimen preparation

This study was performed with approval from the IACUC at Virginia Tech and in accordance with the NIH Guide for the Care and Use of Laboratory Animals. A total of $n = 37$ CD-1 mice (Charles River Laboratories International, Inc.) between 90 and 150 days of age were used in this study. Mice were housed in a biosafety level 1 vivarium with a 12-h light-dark cycle and free access to food and water. The mice were split among three groups: virgin non-pregnant (NP, $n = 13$), mid-pregnant (MP, $n = 11$), and late-pregnant (LP, $n = 13$) (Fig. 1(a)). MP and LP mice were naturally bred using a timed-pregnancy protocol as detailed in prior work [14]. Briefly, once female mice entered the proestrous phase of the murine reproductive cycle as determined by visual inspection of the vaginal opening [34], male mice were introduced

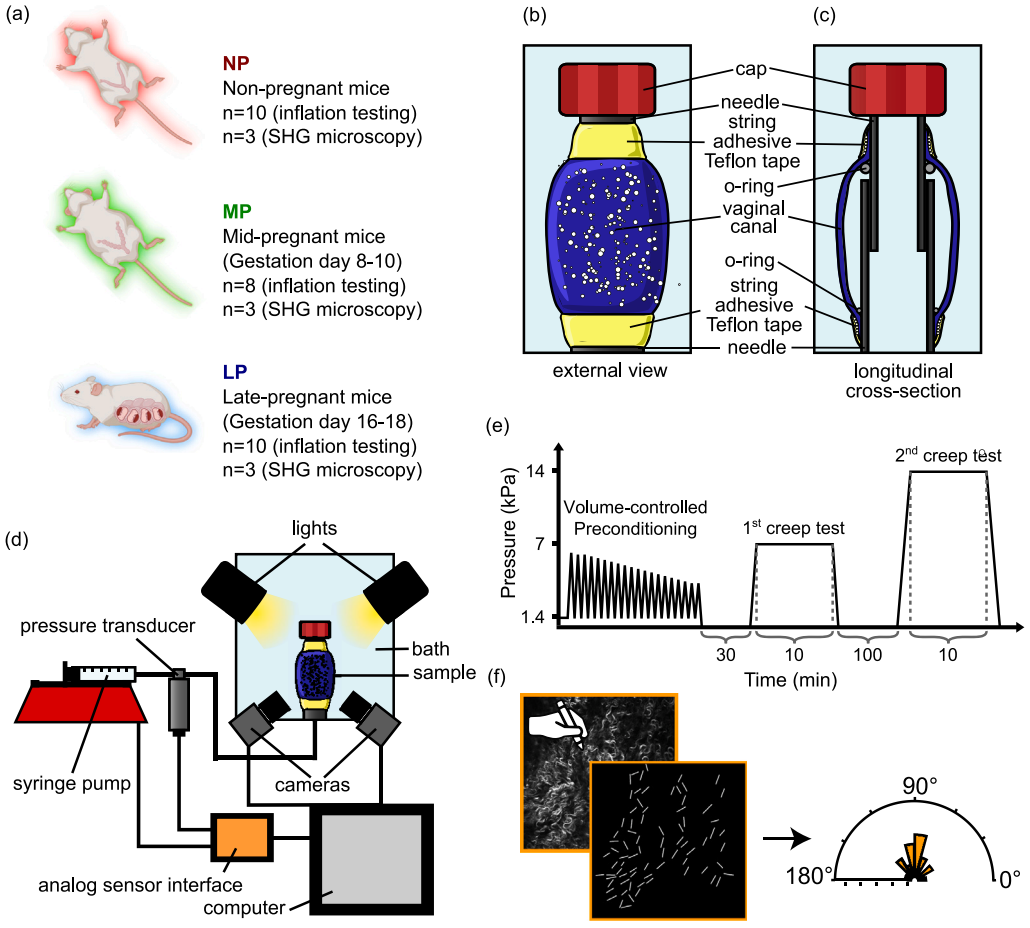

Fig. 1. (a) Overview of the three experimental groups: non-pregnant (NP), mid-pregnant (MP; GD: 8.5–10.5), and late-pregnant (LP; GD: 16.5–18.5) mice. (b–c) Three-dimensional and longitudinal cross-sectional views of the vagina mounted on coaxial needles and speckled for full-field strain measurements. (d) Complete experimental apparatus. (e) Testing protocol, consisting of volume-controlled preconditioning followed by a pre-creep (ramp) test to 7 kPa, a 600 s creep hold at 7 kPa, a 6000 s recovery period, and a second pre-creep (ramp) test to 14 kPa followed by a 600 s creep hold; the time axis is not to scale. (f) Second harmonic generation (SHG) imaging; collagen in the mid-region of vaginal specimens was manually segmented to quantify predominant fiber directions. (For interpretation of the references to color in this figure legend, the reader is referred to the web version of this article.)

into female cages and left overnight. The morning after, female mice were checked for vaginal plugs to determine if copulation occurred. The vaginal plug was observed at gestation day (GD) 0.5, and the progression of pregnancy was subsequently monitored by periodically weighing and visually inspecting the mice for abdominal size and nipple enlargement. MP mice were sacrificed at GD 8.5–10.5, while LP mice were sacrificed at GD 16.5–18.5 (total gestation: 19–20 days). NP mice, never exposed to males, were sacrificed in estrus, as determined by visual inspection of the vaginal opening for color, texture, and gaping [34]. All mice were euthanized via carbon dioxide inhalation, in accordance with American Veterinary Medical Association (AVMA) guidelines. Immediately following euthanasia, mice were refrigerated at 4 °C until dissection for either mechanical testing (NP: $n = 10$, MP: $n = 8$, LP: $n = 10$) or SHG microscopy ($n = 9$, with 3 mice per gestational group). All samples were tested within 48 h of euthanasia and stored in the refrigerated animal carcass until testing. When testing could not be completed on the day of euthanasia, specimens were tested on the following day. Similar post-mortem intervals have been used for mechanical testing of other soft tissues [35,36]; however, to our knowledge, this storage protocol has not been specifically evaluated for vaginal tissue.

2.2. Inflation testing

Vaginal tracts were isolated and prepared for testing as described previously [27]. The whole vagina was dissected, and excess tissue was removed with the exception of the urethra, which could not be removed without substantial risk of damaging the vagina. Cross-sectional images of the proximal end of each vagina were acquired under a microscope using a CMOS camera (Thorlabs Inc., Newton, NJ, USA). From these images, the outer radius and wall thickness of each sample were measured using the path and line drawing tools in ImageJ (NIH, Bethesda, MD, USA). To provide structural support during imaging, each vagina was mounted on the largest flat-tip stainless steel dispensing needle that accommodated the tissue without inducing stretch (6-gauge for MP and LP; 6- or 8-gauge for NP). The mean ± standard deviation (SD) outer radii and wall thicknesses for each group are reported in Table 1.

Samples were subsequently mounted onto concentric needles, as depicted in Fig. 1(b)–(c) and described previously [27,37]. Needle pairs were selected according to tissue size (6/8-gauge for MP and LP; 6/8- or 8/10-gauge for NP), with the distal end of the vagina mounted on the larger needle and the proximal end on the smaller needle. Samples were secured over O-rings using fishing line, N-butyl cyanoacrylate tissue adhesive (Vetbond, 3M, St. Paul, MN, USA), and Teflon tape.

Following mounting, the axial length of each sample was measured using digital calipers (accuracy ±0.1 mm; Mitutoyo Absolute Low Force Calipers Series 573, Kawasaki, Japan) and used to calculate the initial vaginal volume. The mean ± SD axial lengths and initial volumes for each experimental group are reported in Table 1. Samples were then dyed with a 1% methylene blue solution (Fisher Science Education, Nazareth, PA, USA), after which excess dye was rinsed off

Table 1
Mean (±SD) age and weight of the mice, and mean (± SD) outer radius, thickness, length, and inner volume of the vaginal samples from each experimental group.

gestational status	NP	MP	LP
Age (days)	93.5 ± 6.1	114.5 ± 17.5	107.4 ± 10.0
Weight (g)	34.7 ± 5.1	46.3 ± 5.9	63.4 ± 7.6
Outer radius (mm)	2.53 ± 0.29	2.82 ± 0.04	3.02 ± 0.11
Thickness (mm)	0.37 ± 0.07	0.28 ± 0.03	0.41 ± 0.08
Length (mm)	7.84 ± 1.58	7.66 ± 1.47	10.18 ± 1.56
Inner volume (mm^3)	136.9 ± 41.1	173.0 ± 30.9	253.1 ± 35.3

with 1× phosphate-buffered saline (PBS) (MIDSCI, Fenton, MO, USA). The dorsal vaginal wall was subsequently speckled with white spray paint (Rust-Oleum, Vernon Hills, IL, USA) to generate a high-contrast speckle pattern suitable for non-contact strain measurement, a procedure shown to have minimal effect on native tissue mechanics [38]. Throughout all preparation steps, from dissection through speckling, samples were kept hydrated by spraying PBS onto the tissue surface at least once every two minutes.

Experiments were conducted using a custom-built inflation rig (Fig. 1(d)). Immediately following speckling, samples were mounted vertically in a PBS bath at room temperature, with the introitus oriented downward. Samples were connected via plastic tubing to a pressure transducer (maximum capacity: 345 kPa, accuracy ±0.25%, Omega Engineering, Norwalk, CT, USA) and a computer-controlled syringe pump (accuracy ±1%, NE-1000, New Era Pump Systems Inc., Farmingdale, NY, USA). Pressure transducer output was monitored in real time and recorded using a custom MATLAB script (R2018a, MathWorks, Natick, MA, USA) and a myDAQ data acquisition device (accuracy ±0.5%; ±20 mV input range, National Instruments, TX, USA). Samples were preloaded to a luminal pressure of 1.4 kPa, which was selected as the reference configuration for all strain measurements, as this pressure was sufficient to consistently support the weight of the upper needle assembly [27,37]. From this reference configuration, samples were preconditioned to +30% of their initial volume (Table 1) and returned to the reference configuration at a flow rate of 2.0 mL/min for 20 cycles. Following preconditioning, specimens were allowed to recover for 30 min before testing to minimize transient viscoelastic effects. This recovery period was selected based on preliminary experiments demonstrating that two consecutive creep tests up to 14 kPa produced comparable mechanical responses.

Fig. 1(e) illustrates the experimental protocol. From the reference configuration, samples were infused with PBS at a constant volumetric rate of 0.35 mL/min until a luminal pressure of 7 kPa was reached, constituting the first pre-creep test. The pressure was maintained through periodic reinfusion at a rate of 0.08 mL/min for 600 s, constituting the first creep test. PBS was then withdrawn at a rate of 0.35 mL/min until the luminal pressure returned to 1.4 kPa. This pressure was maintained for 6000 s via periodic infusion and/or withdrawal at a rate of 0.1 mL/min, constituting the recovery period. A 10:1 ratio of recovery duration to creep duration has been previously recommended for creep testing [39,40] and has been applied to vaginal specimens in previous studies [26]. Additional recovery time was included to account for the time required to load and unload the tissue. Following recovery, samples were infused at the same constant volumetric rate until a luminal pressure of 14 kPa was reached, constituting the second pre-creep test. This pressure was again maintained through periodic reinfusion at a rate of 0.08 mL/min for 600 s, constituting the second creep test. The selected creep pressures fall within the range of peak uterine pressures reported during the second stage of labor [23]. Throughout the creep and recovery periods, luminal pressure was maintained by a feedback-controlled system using an analog sensor interface (Ana-Box Model ADPT-ANABOX-11, New Era Pump Systems Inc., Farmingdale, NY, USA).

High-definition images (2448 × 2048 pixels) of the dorsal wall of the vaginas were captured using two CMOS cameras (CSI-acA2440, Correlated Solutions, Columbia, SC, USA) equipped with C-mount lenses (Xenoplan 2.8/50, Schneider Optics Inc., Hauppauge, NY, USA). During loading at a volumetric flow rate of 0.35 mL/min, images were acquired at 4 Hz, while during creep the acquisition rate was reduced to 0.4 Hz. The acquired images were used to perform non-contact strain measurements using a three-dimensional DIC system (strain resolution $> 10\mu\epsilon$, Vic-3D 10, Correlated Solutions, Columbia, SC, USA). Camera calibration for DIC was performed using a through-light calibration grid (4-in-1, 9 × 9 dot calibration target, 0.89 mm spacing, Correlated Solutions, Columbia, SC, USA).

2.3. Mechanical data

Maps of the local normal Lagrangian strains in the LD and CD across the surface of each sample were obtained using the DIC system throughout testing. These strains were defined relative to a reference configuration corresponding to the loaded state at a luminal pressure of 1.4 kPa, measured during the first inflation up to 7 kPa. From these strain maps, average strain values were computed within a small circular region of interest located at the mid-vagina and away from the clamped ends and any regions of high correlation error or speckle degradation. These locally averaged normal strain values were taken as representative of each specimen and are hereafter referred to as the LD and CD strains.

Tangent compliances during each pre-creep phase were estimated by numerically differentiating strain with respect to pressure in each direction using the `gradient` function in MATLAB. Tangent compliance, therefore, quantifies the pressure-normalized deformation of the region of interest in response to an incremental increase in luminal pressure. The values immediately preceding the end of each pre-creep phase were taken as the tangent compliances in the LD and CD. Because this derivative was computed with respect to pressure rather than wall stress, tangent compliance should be interpreted as a measure of the organ-level mechanical response rather than an intrinsic material property.

For each sample, the initial strains for the first and second creep tests were defined as the LD and CD strains at the moment when the nominal creep pressures of 7 kPa and 14 kPa, respectively, were first reached during inflation. Changes in strain during the first creep test were calculated by subtracting the initial strain values at the beginning of the test from the strain values at subsequent times. An analogous procedure was used to calculate strain changes in each direction during the second creep test.

2.4. Statistical analysis of mechanical data

Statistical analysis was performed using RStudio (Build 563, Posit Software, PBC, Boston, MA). Tangent compliances at the end of each pre-creep phase were analyzed using a three-way mixed-model analysis of variance (ANOVA), with gestational status (NP, MP, LP) as a between-subjects factor and anatomical direction (LD, CD) and test order (first and second, conducted up to 7 kPa and 14 kPa, respectively) as within-subjects factors. Normality was assessed using the Shapiro–Wilk test; tangent compliance values in the CD during the second pre-creep test for the LP group were not normally distributed, so they were square-root-transformed to satisfy the normality assumption. Changes in strain at $t = 600$ s during each creep test were analyzed using an analogous three-way mixed-model ANOVA. Several strain datasets did not meet the assumption of normality, and no transformation successfully normalized all groups; therefore, strain analyses are reported using the original, non-transformed data. Greenhouse–Geisser corrections were applied when the sphericity assumption was violated. No significant three-way interactions were observed. Significant two-way interactions were followed by simple main effects analyses,

while main effects were evaluated directly when no interactions were present. Repeated-measures one-way ANOVA was used for within-subjects factors and standard one-way ANOVA for between-subjects factors. Post-hoc pairwise comparisons were performed using Holm–Bonferroni corrections. Statistical significance was defined as $p < 0.05$, and data are reported as mean ± standard error of the mean (SEM).

2.5. SHG microscopy

Collagen microstructure was examined using SHG imaging in each experimental group (NP, MP, and LP; $n = 3$ mice per group), following previously established protocols [41]. The SHG analysis was initiated following the mechanical testing to further interpret the experimental findings; consequently, specimen availability was limited. Tissue collection and dissection procedures were identical to those used for mechanical testing. Imaging was performed using an LSM 880 multiphoton microscope (Zeiss, Thornwood, NY, USA) equipped with a Ti:Sapphire laser (Ultra 1, Coherent Inc., Santa Clara, CA, USA) tuned to 780 nm and a 20× water-immersion objective.

Each vaginal specimen was placed in a polydimethylsiloxane (PDMS) mold, submerged in PBS, and covered with a coverslip as described by Huntington et al. [42]. The mid-vaginal region on the dorsal exterior surface was imaged near the center of the tissue and away from the edges, corresponding spatially to the region of interest used for DIC-based strain analysis. Images covered an area of 425 × 425 μm, and two consecutive image planes separated by 10 μm in the radial direction of the vagina were acquired for each specimen.

To quantify collagen fiber orientation, a blinded observer manually traced the centerlines of 50 collagen fibers per image to represent the predominant fiber directions. Manual tracing was necessary because curved fibers were frequently segmented into multiple fragments, causing a single collagen fiber to be represented by multiple orientation angles. The traced overlays were binarized in ImageJ (NIH, Bethesda, MD, USA) and imported into CurveAlign to automatically extract the orientation angle of each traced fiber. In this convention, 0°/180° corresponds to the CD and 90° corresponds to the LD.

2.6. Statistical analysis of SHG data

Fiber orientation angles were analyzed in RStudio, with angle counts normalized to probability distributions using consistent histogram binning. For each specimen, the binned angle distributions from the two image planes were averaged to generate a representative orientation distribution. Circular statistics, including the circular mean ± SEM and circular variance, were computed for each gestational group. Watson's test was used to assess deviations from a uniform circular distribution. Differences in fiber orientation distributions across gestational groups were evaluated using the Watson–Williams test, with Bonferroni corrections applied for multiple comparisons. Circular variance was assessed for normality using the Shapiro–Wilk test and for homogeneity of variance using Levene's test. One-way ANOVA was used to evaluate differences in circular variance across gestational groups.

3. Results

Strain fields were spatially heterogeneous across the dorsal surface of each specimen throughout inflation testing, including both the pre-creep and creep phases of the protocol (Fig. 1(e)). To enable consistent quantitative comparisons, strain measurements were extracted from a fixed circular region of interest at the mid-vaginal exterior surface for all samples. Representative strain maps illustrating this spatial heterogeneity are shown in Fig. 2(a) for NP, MP, and LP samples. The corresponding representative CD strain histories, including the ramp to the target pressure and the subsequent creep response, are shown in Fig. 2(b). For all specimens, strain increased rapidly during inflation to the target creep pressure and subsequently evolved more gradually under constant pressure during the creep phase. Due to their larger initial volumes (Table 1), LP samples required a longer inflation period to reach the target pressure than NP and MP samples; however, inflation duration was less than 20 s for all specimens, representing less than 5% of the total creep duration 600 s. Minor fluctuations in strain observed during creep were attributed to small pressure variations associated with periodic PBS reinfusion required to maintain constant pressure (Fig. 2(b)).

The pressure–strain responses during inflation to the first and second creep pressures in the LD and CD are shown in Fig. 3, with individual samples grouped by gestational status. Within each group, variability in mechanical response is evident, with some specimens exhibiting larger strains than others at the same applied pressure. Across all groups, strains were consistently greater in the CD than in the LD. From the reference configuration at 1.4 kPa to the target creep pressures of 7 and 14 kPa, samples exhibited a nonlinear increase in strain with increasing pressure, with more pronounced nonlinearity at lower pressures. The pressure–strain responses up to 7 kPa were generally similar between the first (Fig. 3(a–f)) and second tests (Fig. 3(g–l)); however, modest deviations were observed in the second test because the tissue did not fully recover after returning to the preload pressure of 1.4 kPa, resulting in nonzero starting strains.

Tangent compliance values at the end of each pre-creep inflation phase are reported in Fig. 4. Factorial mixed-model ANOVA revealed no significant two-way or three-way interactions among gestational status, anatomical direction, and test order. Significant main effects were observed for all three factors. When data were pooled across gestational groups and anatomical directions (Fig. 4(a)), tangent compliances measured during the second pre-creep test were significantly lower than those measured during the first pre-creep test ($p < 0.001$). When data were pooled across gestational groups and test order (Fig. 4(b)), tangent compliances in the CD were significantly greater than those in the LD ($p < 0.001$). When data were pooled across anatomical directions and test order (Fig. 4(c)), post-hoc analysis identified significant differences between the LP and MP groups ($p = 0.015$). A difference between the NP and MP groups was observed in the original dataset ($p = 0.020$), but this comparison did not reach statistical significance following transformation ($p = 0.052$). No significant differences were observed between the NP and LP groups ($p = 0.425$).

The temporal evolution of strain during each creep test in the LD and CD is shown in Fig. 5, with individual samples grouped by gestational status. Across all groups, strain generally increased nonlinearly with time during creep, with higher creep rates observed early in the creep phase. In many specimens, strain increased during the initial portion of creep (typically within the first 60 s) before partially decreasing, whereas other specimens exhibited monotonic decreases in strain in one anatomical direction. Negative changes in strain during creep were observed in a subset of NP and MP samples. During the first creep test, negative strain changes occurred in the LD for two NP samples (Fig. 5(a)) and one MP sample (Fig. 5(b)), and in the CD for one NP sample (Fig. 5(d)). Such behavior was more prevalent during the second creep test. In the NP group, three samples exhibited negative strain changes in the LD (Fig. 5(g)) and three different samples exhibited negative strain changes in the CD (Fig. 5(j)). In the MP group, one sample exhibited a negative strain change in the LD during the second creep test (Fig. 5(h)). No LP samples exhibited negative strain changes during creep in either direction (Fig. 5(c,f,i,l)). Across all gestational groups, no specimen exhibited decreases in strain simultaneously in both directions during a single creep test. Although individual specimens often exhibited greater creep in one anatomical direction than the other, the overall magnitudes of strain change in the LD and CD were comparable across gestational groups.

Changes in LD and CD strain at 600 s into each creep test are plotted in Fig. 6. By factorial ANOVA, a significant interaction was observed between gestational status and creep test order (test 1 vs. test

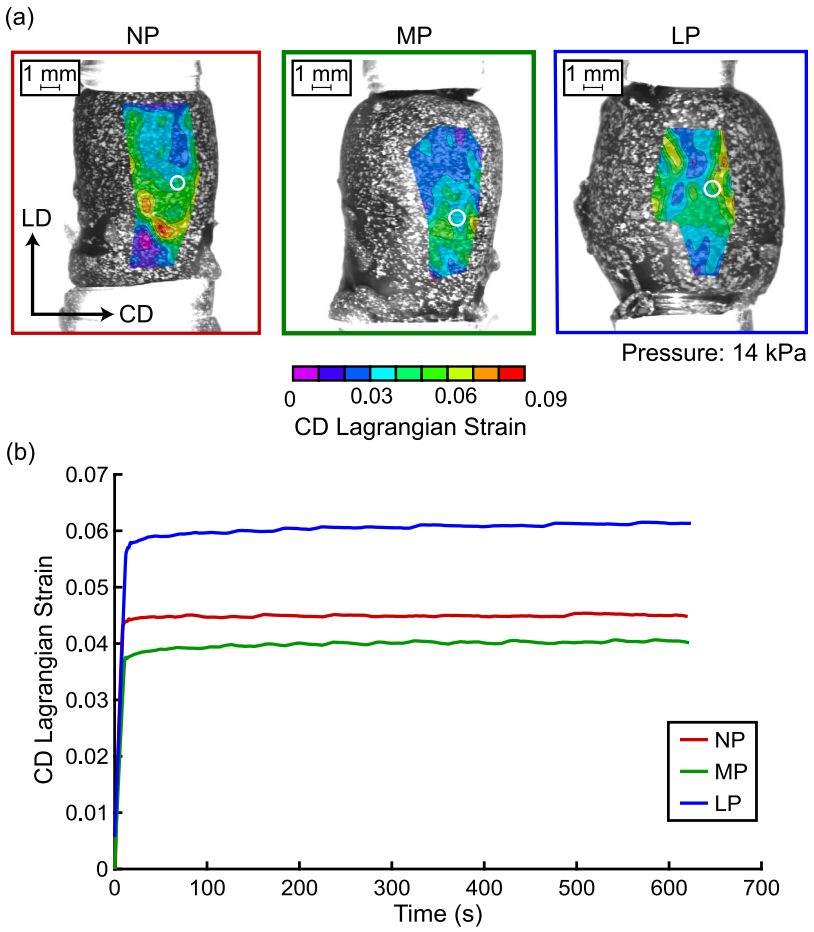

Fig. 2. Representative experimental results illustrating the spatial and temporal strain response during inflation testing for one specimen from each gestational group: non-pregnant (NP), mid-pregnant (MP), and late-pregnant (LP). (a) Circumferential (CD) Lagrangian strain fields at the onset of the creep test; white circles indicate the region of interest used for strain quantification. (b) Representative CD strain–time histories during inflation from 1.4 kPa to 14 kPa, followed by a 600 s creep hold. (For interpretation of the references to color in this figure legend, the reader is referred to the web version of this article.)

2) ($p = 0.033$). When data were pooled across anatomical directions, strain changes during the first creep test were significantly greater than those during the second creep test in the NP ($p < 0.001$) and LP ($p = 0.016$) groups (Fig. 6(a)). No significant difference between the first and second creep tests was observed in the MP group ($p = 0.342$). Gestational status showed a significant simple main effect in both the first and second creep tests (test 1: $p = 0.013$; test 2: $p = 0.012$). Post-hoc analysis indicated that, during the first creep test, strain changes in the LP group were significantly greater than those in the MP group ($p = 0.014$; Fig. 6(b)). During the second creep test, strain changes in the LP group were significantly greater than those in the NP group ($p = 0.022$; Fig. 6(b)). All other pairwise comparisons were not statistically significant ($p \geq 0.05$). No significant interactions or main effects involving anatomical direction were observed.

Following observations of pregnancy-associated changes in tangent compliance and creep strain, a pilot study was conducted to examine the collagen microstructure and elucidate the underlying structural basis of these changes. Representative SHG images of the external surface of the murine vagina are depicted in Fig. 7(a). Qualitatively, collagen in the NP group appeared crimped with a modest preferential alignment to the LD (Fig. 7(b)). At MP, the collagen fibers appeared more disorganized, with a greater fraction oriented toward the CD (Fig. 7(b)). In this group, the fiber crimp exhibited a less uniform wave pattern across the field of view than in the NP group. Collagen fibers in LP vaginas appeared more densely packed, with more uniform and relaxed crimp than in the earlier gestational stages. At this stage, collagen fibers also appeared to exhibit greater alignment with the LD.

The distributions of collagen fiber alignment for each specimen at each gestational stage are shown in Fig. 7(b). The circular mean direction of the collagen fibers was 73.32° for NP, 102.74° for MP, and 66.95° for LP (Fig. 7(c)). A Watson–Williams test indicated a significant difference in mean direction among gestational groups ($p < 0.001$). Post hoc pairwise comparisons showed that NP differed from MP ($p < 0.001$) and MP differed from LP ($p < 0.001$), whereas NP and LP did not differ ($p = 1.0$). The mean circular variance (± SEM) of fiber directions was 0.261 (0.025) for NP, 0.384 (0.0098) for MP, and 0.202 (0.0245) for LP (Fig. 7(d)). The relatively high circular variance of the MP group indicates a broad distribution of fiber orientations. Consequently, the circular mean represents the average orientation across all fibers and does not necessarily coincide with the most prominent peak in the corresponding orientation histogram. A one-way ANOVA indicated a significant effect of gestational stage on circular variance ($p = 0.032$). Post hoc comparisons with Bonferroni correction revealed a difference between MP and LP ($p = 0.037$), while NP did not differ from either MP ($p = 0.16$) or LP ($p = 0.90$).

4. Discussion

This study demonstrates that the mechanical behavior of the vagina changes systematically across gestation and depends on both loading magnitude and loading duration. Using biaxial inflation with volume ramp loading and subsequent constant-pressure creep, we found that *the intact murine vagina exhibits lower compliance at mid-pregnancy* than

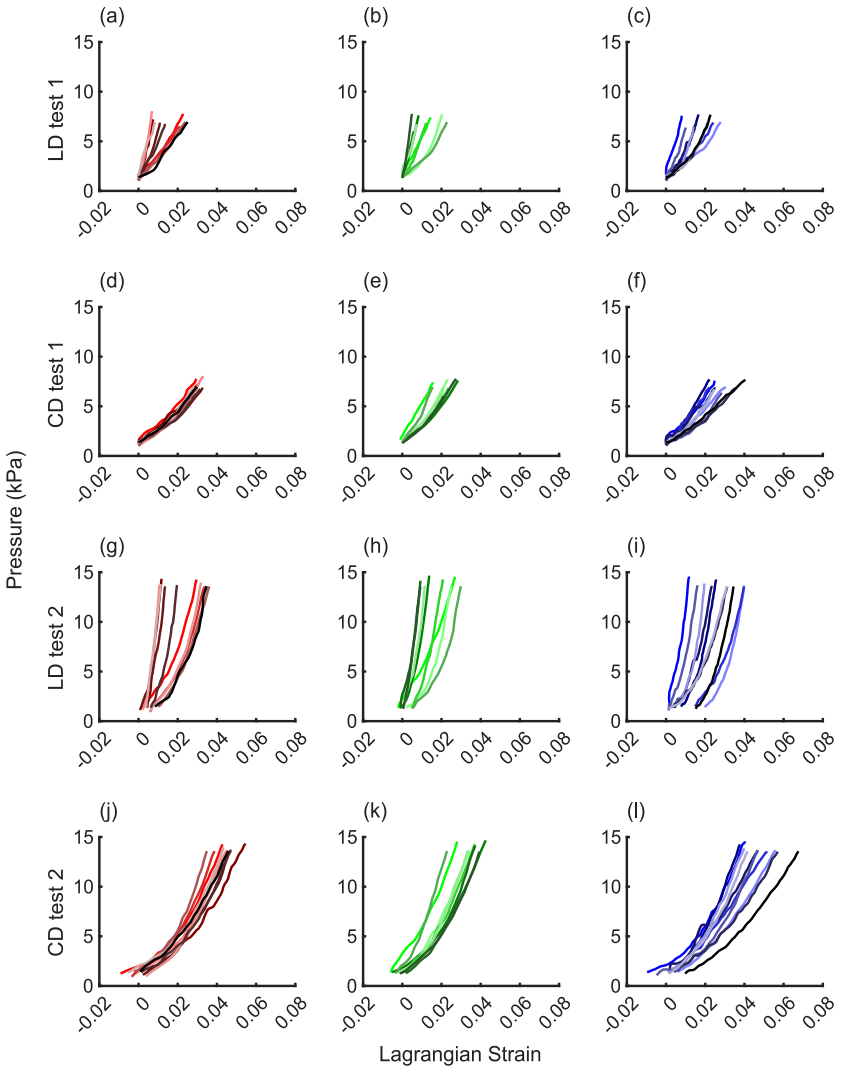

Fig. 3. Pressure–strain responses during inflation up to the first (test 1, up to 7 kPa) and second (test 2, up to 14 kPa) creep pressures for $n = 10$ non-pregnant (NP), $n = 8$ mid-pregnant (MP), and $n = 10$ late-pregnant (LP) specimens. Panels are organized by anatomical direction, longitudinal (LD) and circumferential (CD), and test order, with rows from top to bottom corresponding to LD test 1, CD test 1, LD test 2, and CD test 2, and columns corresponding to NP (red curves), MP (green curves), and LP (blue curves) groups. Each curve represents an individual specimen, with consistent color shading used to track data from the same specimen across panels. (For interpretation of the references to color in this figure legend, the reader is referred to the web version of this article.)

in the NP and LP states, while *the LP vagina exhibits greater time-dependent deformation during constant loading*. These findings indicate *a transient reduction in compliance* during early to mid-pregnancy, followed by increased time-dependent deformation under constant loading near term. The greater deformation observed in the late-pregnant vagina is consistent with recent inflation testing of the intact murine reproductive tract, which demonstrated increased distensibility of the reproductive tract during late pregnancy together with region-specific deformation under pressure [33]. Our SHG analysis indicated a shift in mean collagen fiber direction and a broader distribution of fiber orientations at mid-pregnancy, followed by a more aligned organization and return toward the non-pregnant orientation at late pregnancy. Collectively, these data show that pregnancy modulates not only the magnitude of vaginal deformation but also the timing and loading conditions under which it develops, with concurrent changes in collagen organization.

Across all gestational groups, vaginal specimens exhibited a nonlinear pressure–strain response in both the LD and CD (Fig. 3). Such nonlinearity is consistent with progressive collagen fiber recruitment, a mechanism commonly invoked to explain the toe region observed in soft connective tissues under uniaxial loading [43]. In the vagina, collagen fibers are initially wavy (as can be seen in our SHG images in Fig. 7(a)), and they likely do not contribute substantially to load bearing until they become straight. As pressure increases, fibers straighten and become engaged, leading to an increase in tissue stiffness [41]. This gradual recruitment provides a mechanistic explanation for the nonlinear inflation response observed in all our specimens across gestation stages.

Despite similar qualitative nonlinearity, the magnitude of deformation differed with gestational stage. MP samples were less compliant than both NP and LP samples, indicating greater resistance to deformation during inflation at early to mid-pregnancy (Fig. 4). Similar gestation-dependent stiffening has been reported in the murine cervix through early- to mid-pregnancy [44–47], where increased tissue stiffness is thought to support structural integrity and contribute to maintaining pregnancy by resisting premature deformation [48]. A comparable functional role likely exists for the vagina, which is not required to undergo large deformations during mid-pregnancy, as sexual receptivity is suppressed and large deformations are primarily associated with copulation or delivery [49]. In this context, increased vaginal stiffness may also contribute to supporting the cervix, to which it is mechanically coupled, helping to resist premature deformation and reduce the risk of preterm birth.

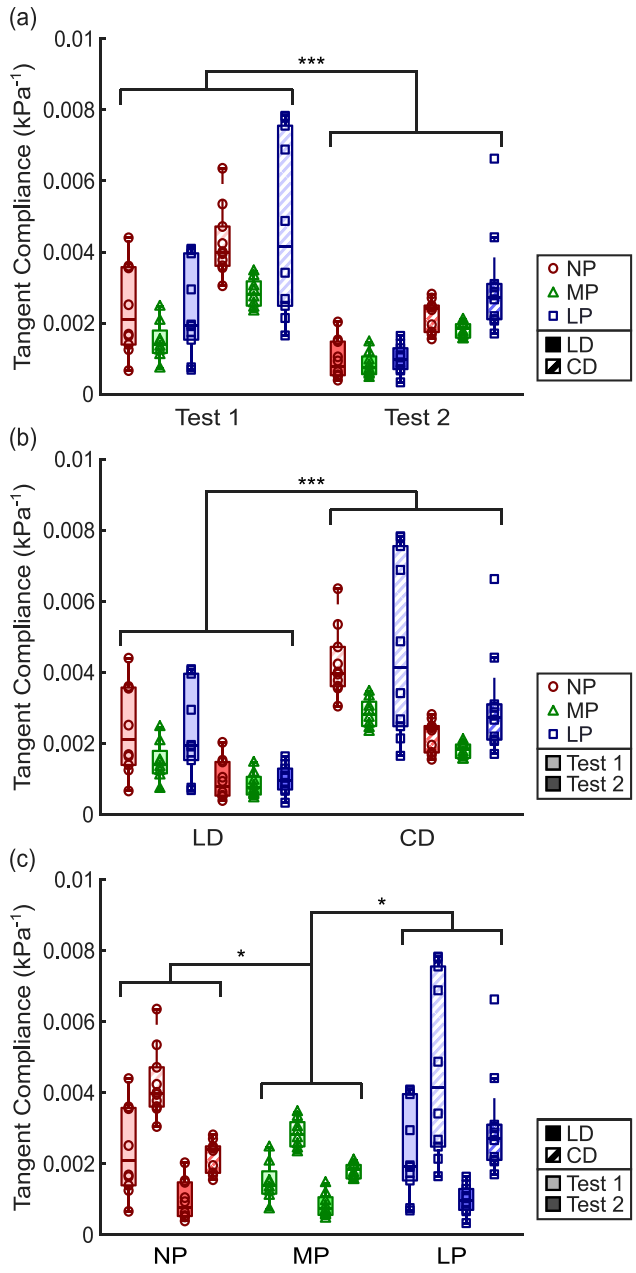

Fig. 4. Tangent compliances for non-pregnant (NP), mid-pregnant (MP), and late-pregnant (LP) groups, separated by anatomical direction, longitudinal (LD) and circumferential (CD), and test order (test 1 up to 7 kPa and test 2 up to 14 kPa). (a) Data grouped by test order. (b) The same data grouped by anatomical direction. (c) The same data grouped by gestational status. Individual specimen values are shown as markers, with boxes indicating the median and interquartile range. $*p < 0.05$, $***p < 0.001$. (For interpretation of the references to color in this figure legend, the reader is referred to the web version of this article.)

LP tissue exhibited greater time-dependent deformation under constant pressure (Fig. 6). By the end of the creep period, LP samples underwent greater strain than MP samples at lower pressures and greater strain than NP samples at higher pressures, indicating a load-dependent modulation of time-dependent mechanical response across gestation. These findings suggest that late-gestation remodeling does not simply soften the tissue but instead alters how deformation evolves over time. The dependence on pressure further indicates that different deformation mechanisms are likely engaged across loading regimes, with lower pressures probing early stages of fiber engagement and higher pressures reflecting the response of the fully recruited collagen network. Such load-dependent viscoelastic adaptation is consistent with the functional demands of parturition, during which the vagina must accommodate large, sustained deformations under prolonged loading. By redistributing stresses over time through progressive recruitment of collagen fibers, these adaptations likely reduce susceptibility to tissue injury during delivery.

SHG imaging revealed gestation-dependent alterations in collagen architecture, including a transient shift in mean fiber orientation and increased fiber dispersion at mid-pregnancy (Fig. 7). These structural changes may influence load distribution and collagen fiber recruitment during inflation, contributing to the transient reduction in compliance observed at this stage. By late pregnancy, collagen organization shifted toward the non-pregnant state, suggesting continued remodeling of the extracellular matrix as the mechanical demands of gestation evolved. These findings are consistent with previous studies of the murine cervix, which have reported stage-specific changes in collagen organization and tissue mechanics during early to mid-gestation [50]. Although collagen density and turnover were not quantified in the present study, alterations in collagen architecture, together with potential changes in other extracellular matrix constituents, likely contribute to the evolving mechanical response [17]. The SHG analysis was performed on a limited subset of specimens and, therefore, should be interpreted as complementary to the mechanical data. Systematic characterization of vaginal extracellular matrix organization throughout gestation remains limited [17], and further studies that combine quantitative imaging with mechanical testing are needed to elucidate the microstructural mechanisms underlying these biomechanical adaptations.

Several NP and MP samples exhibited negative strain changes in one anatomical direction during creep (Fig. 5), indicating strong mechanical coupling between the LD and CD. In these cases, extension in one direction was accompanied by compensatory contraction in the orthogonal direction. The precise mechanism underlying the observed negative strain changes was not investigated in the present study. However, the behavior is consistent with strong mechanical coupling between the LD and CD arising from the anisotropic mechanical behavior of the vaginal tissue, whereby load redistribution during creep may permit increasing deformation in one direction while strain decreases in the orthogonal direction under constant applied pressure. In contrast, the limited occurrence of negative strain changes in LP samples suggests that gestation-dependent remodeling alters this directional constraint and promotes positive strain in both anatomical directions under constant loading. LP tissue exhibited lower circular variance relative to MP samples, indicating greater collagen fiber alignment (Fig. 7(d)). This change in structure may alter the distribution of strain between the LD and CD under biaxial inflation, reducing the tendency for negative strain to develop in one direction as the other undergoes extension. Such coordinated deformation may facilitate expansion of the vagina during fetal passage.

We did not observe significant differences in compliance between the NP and LP vaginas, in contrast to prior animal studies reporting decreased stiffness in late pregnancy [15,16,18–20,30]; see also Figure 5 in Dubik et al. [10]. Moreover, our finding that the MP vagina exhibited lower compliance than both the NP and LP groups differs from the results of Feola et al. [31], the only other study to mechanically evaluate the vagina at mid-pregnancy. Using uniaxial tensile testing of longitudinal vaginal specimens, Feola et al. reported a significant decrease in tangent modulus during mid-pregnancy, indicating increased tissue distensibility relative to the non-pregnant state. These differences may, in part, reflect the distinct loading configurations and mechanical measures employed. In the present study, compliance was quantified from the local pressure–strain response measured using DIC during inflation testing. In contrast, previous studies have primarily characterized mechanical behavior using uniaxial load–displacement or

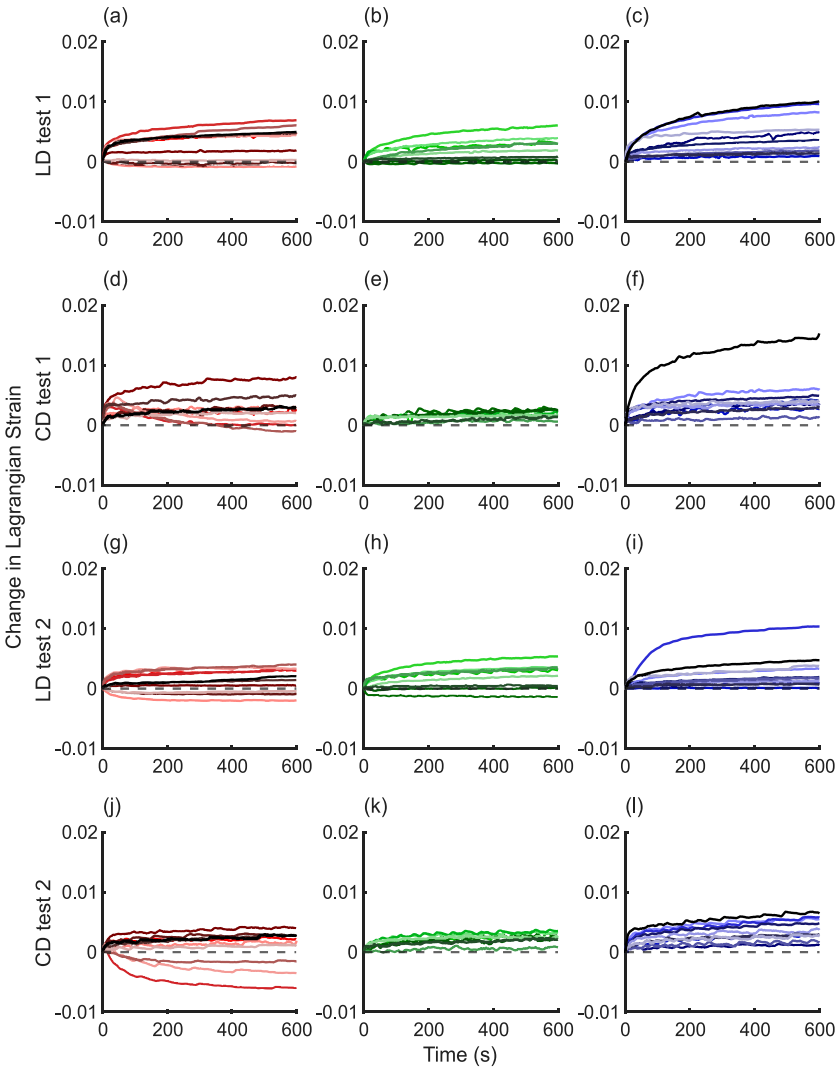

Fig. 5. Changes in strain throughout the first (test 1, at 7 kPa) and second (test 2, at 14 kPa) creep tests for $n = 10$ non-pregnant (NP), $n = 8$ mid-pregnant (MP), and $n = 10$ late-pregnant (LP) specimens. Panels are organized by anatomical direction, longitudinal (LD) and circumferential (CD), and test order, with rows from top to bottom corresponding to LD test 1, CD test 1, LD test 2, and CD test 2, and columns corresponding to NP (red curves), MP (green curves), and LP (blue curves) groups. Each curve represents an individual specimen, with consistent color shading used to track data from the same specimen across panels. (For interpretation of the references to color in this figure legend, the reader is referred to the web version of this article.)

stress–strain responses, or from global pressure–volume measurements, which do not resolve local tissue deformation.

One limitation of the present study is that the second creep test was performed after completion of the first creep test, rather than being conducted independently following a separate preconditioning sequence. Although all specimens underwent the same standardized volume-controlled preconditioning, 30-min recovery period, and testing protocol, loading-history-dependent effects cannot be completely excluded when comparing the responses between the two creep tests. Nevertheless, the recovery period was selected based on preliminary experiments demonstrating that two consecutive creep tests up to 14 kPa produced comparable mechanical responses. Future studies could investigate alternative protocols, including independently preconditioning specimens before each loading condition, to further isolate loading-history effects.

The MP and LP groups encompassed gestational windows of GD 8.5–10.5 and GD 16.5–18.5, respectively. Given that murine gestation spans only approximately 20 days, differences in the exact gestational day at sacrifice may have introduced biological variability within each group. Nevertheless, similar gestational windows have been adopted in previous studies of pregnancy-induced vaginal remodeling in rats [20, 30–32]. The observed non-monotonic changes suggest that pregnancy-induced vaginal remodeling does not progress uniformly throughout gestation but instead involves stage-specific mechanical adaptations. Narrower gestational windows in future studies may, therefore, provide greater insight into the temporal evolution of vaginal biomechanical adaptation.

The DIC method was used to obtain full-field strain measurements across the exposed dorsal surface of the murine vagina. Although strain fields were computed over the entire visible surface, quantitative analyses were restricted to a region of interest within the mid-vaginal segment to provide consistent strain measurements while minimizing boundary effects associated with specimen mounting. Consequently, the reported strains characterize deformation within this region and should not be interpreted as representing the overall specimen response or intrinsic material behavior. Although the selected region of interest was chosen to approximate the average deformation of the specimen, local differences in geometry, collagen architecture, and deformation patterns may have influenced the measured strains. The limited size of the murine vagina, together with inter-specimen variability in geometry, precluded consistent sampling of the proximal and distal regions across all specimens. These regions are also located near the clamped

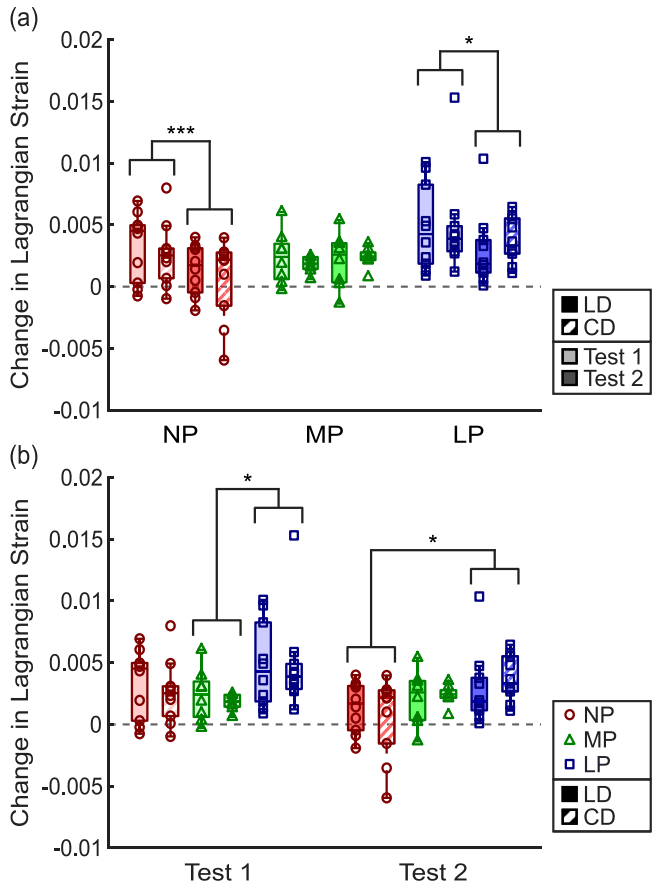

Fig. 6. Changes in strain measured at 600 s during the first (test 1, at 7 kPa) and second (test 2, at 14 kPa) creep tests for all specimens. Results are organized by gestational status, including non-pregnant (NP), mid-pregnant (MP), and late-pregnant (LP) groups, anatomical direction, including longitudinal (LD) and circumferential (CD), and test order. (a) Data grouped by gestational status. (b) The same data grouped by creep test order. Individual specimen values are shown as markers, with boxes indicating the median and interquartile range. $*p < 0.05$, $***p < 0.001$. (For interpretation of the references to color in this figure legend, the reader is referred to the web version of this article.)

boundaries, where stress concentrations and boundary effects may affect the measured response. Future studies may extend this approach using panoramic DIC to characterize regional deformation across the dorsal, lateral, and ventral vaginal walls [51]. The use of larger animal models may further improve spatial resolution along the vaginal length, enabling more comprehensive characterization of regional deformation while reducing the relative influence of mounting and boundary effects. Such studies would also help determine whether the regional variations in vaginal mechanical behavior reported previously [16,52,53] are reflected in local strain patterns during inflation.

The experimental characterization of pregnancy-related biomechanical changes in the human vagina is challenging. Consequently, preclinical animal models are essential for studying these changes [10]. However, important interspecies differences in reproductive biology, such as the frequency of multiple gestations [54], the duration of gestation [55], the timing of progesterone signaling [56,57], and differences in fetal head-to-body size and cephalopelvic proportions [58], must be considered when translating findings to human physiology. These factors likely affect both the time scale and magnitude of pregnancy-induced mechanical and microstructural changes. Although biomechanical testing of pregnant human vaginas is limited by sample availability and experimental control, similarities in microstructural organization across mammals [13] allow findings from animal models to inform human mechanical behavior. Future studies should integrate imaging techniques with mechanical testing to establish direct links between microstructural features (e.g., collagen fiber orientation, waviness, and organization) and mechanical response. For example, integrating instant polarized light microscopy with planar biaxial testing [59] could provide direct characterization of structure–function relationships in the vagina. These approaches will improve our understanding of pregnancy-induced vaginal remodeling and facilitate the translation of these findings to humans.

The present study characterizes the time-dependent mechanical behavior of the vagina across multiple stages of gestation. Although only a limited number of constitutive models have been developed to describe vaginal viscoelasticity under stress relaxation [24] and creep [60], the current dataset provides an opportunity to further develop and validate such models in the context of pregnancy-induced remodeling. Constitutive modeling could provide a quantitative framework for interpreting the observed stage-specific mechanical behavior and relating it to changes in tissue structure and composition. Such models would also facilitate direct comparisons among gestational groups and establish mechanistic links between tissue-scale mechanical behavior and extracellular matrix remodeling. Once validated across multiple stages of gestation, they could be incorporated into computational frameworks to improve predictions of vaginal mechanics throughout pregnancy and support future computational studies of maternal tissue adaptation [61,62].

The observed changes in mechanical behavior noted in this study, together with alterations in collagen organization, suggest structure–function relationships that are likely conserved across species and relevant to human vaginal adaptation. While similarities between murine and human vagina have been reported, reliance on any single animal model is insufficient to capture human physiology, and integration of experimental and computational approaches with human-relevant data will be essential to strengthen translational relevance. One limitation of the present study, consistent with current modeling frameworks, is the lack of representation of active deformations driven by smooth muscle contraction. Smooth muscle activity influences vaginal mechanical response [9,63,64], yet its interaction with pregnancy [31] and viscoelasticity [28,29] remains poorly understood. Incorporating both passive collagen-driven and active smooth muscle-driven deformations will be essential for developing higher-fidelity models that more closely represent vaginal behavior in humans during pregnancy, ultimately supporting improved diagnosis and clinical care in maternal health.

5. Conclusions

This experimental study provides the first characterization of vaginal viscoelasticity across multiple stages of gestation in a murine model. By inflating the vagina to controlled pressures and holding the load constant, we measured tissue strains in the longitudinal and circumferential directions and tracked their evolution over time using the DIC method. As pressure increased, vaginal specimens showed a nonlinear increase in strain, with significantly larger strains in the CD. Notably, specimens from MP animals deformed less than those from NP and LP animals, suggesting that the vagina becomes stiffer during early to mid-pregnancy and then becomes more compliant again near term. At the end of the creep period (600 s), late-pregnant tissue exhibited larger time-dependent strains than mid-pregnant tissue during the first creep test, and larger strains than non-pregnant tissue during the second creep test. These mechanical changes are associated with microstructural remodeling of the tissue, including alterations in collagen organization, as suggested by preliminary SHG imaging. Collagen fibers appeared more dispersed at mid-pregnancy and more aligned at late pregnancy, which may influence load distribution and fiber recruitment, consistent with reduced deformation at mid-pregnancy and increased time-dependent deformation near term. Such remodeling may enable the vagina to withstand larger deformations over time

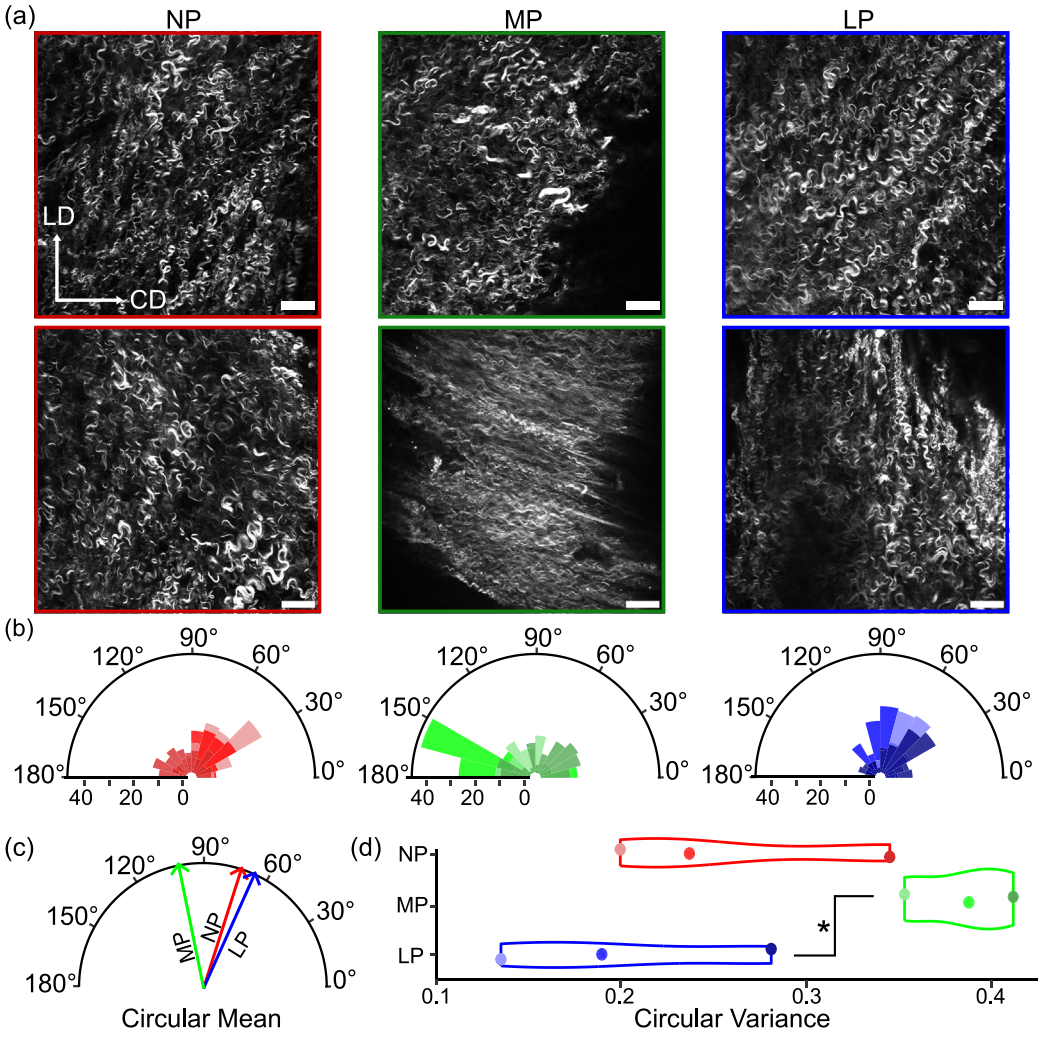

Fig. 7. (a) Second harmonic generation (SHG) images of collagen on the external surface of the murine vagina from non-pregnant (NP), mid-pregnant (MP), and late-pregnant (LP) mice. The arrows shown in the upper-left panel indicate the longitudinal direction (LD) and circumferential direction (CD) for all images, which are oriented from posterior (top) to anterior (bottom). Each image is from a different specimen. Scale bar: 50 μm. (b) Rose plots showing the distribution of collagen fiber orientations for each gestational group. An angle of 90° corresponds to the LD. Bar length represents the normalized fraction of fibers within each orientation bin, and colors distinguish individual specimens ($n = 3$ per group). (c) Circular mean fiber orientation for each gestational group. (d) Circular variance of fiber orientation for each specimen. $^*p < 0.05$. (For interpretation of the references to color in this figure legend, the reader is referred to the web version of this article.)

under prolonged loads, without injury, consistent with the mechanical demands of vaginal birth. Overall, these results establish a foundation for future experimental studies and computational models of vaginal mechanics, with potential relevance for informing improved clinical approaches in maternal care.

CRediT authorship contribution statement

Justin Dubik: Writing – review & editing, Writing – original draft, Visualization, Validation, Methodology, Investigation, Formal analysis, Data curation. **Aileen Suarez:** Writing – review & editing, Writing – original draft, Visualization, Methodology, Investigation, Formal analysis, Data curation. **David Dillard:** Writing – review & editing, Writing – original draft, Supervision, Methodology, Investigation, Formal analysis. **Pamela Moalli:** Writing – review & editing, Investigation. **Raffaella De Vita:** Writing – review & editing, Writing – original draft, Visualization, Supervision, Software, Resources, Project administration, Funding acquisition, Conceptualization.

Declaration of competing interest

The authors declare that they have no known competing financial interests or personal relationships that could have appeared to influence the work reported in this paper.

Acknowledgment

This work was supported by the National Science Foundation under grant number 2053851.

References

[1] C. Phillips, A. Monga, Childbirth and the pelvic floor: "The gynaecological consequences", Rev. Gynaecol. Pract. 5 (1) (2005) 15–22.
[2] J.A. Martin, B.E. Hamilton, M.J.K. Osterman, Births in the United States, 2023, National Center for Health Statistics Data Brief 507, 2024.
[3] J.M. Wu, C.P. Vaughan, P.S. Goode, D.T. Redden, K.L. Burgio, H.E. Richter, A.D. Markland, Prevalence and trends of symptomatic pelvic floor disorders in US women, Obs. Gynecol. 123 (1) (2014) 141.
[4] M.J.K. Osterman, B.E. Hamilton, J.A. Martin, A.K. Driscoll, C.P. Valenzuela, Births: Final data for 2021, Natl. Vital Stat. Rep. 72 (1) (2023) 1–53.

[5] E.M. Skinner, H.P. Dietz, Psychological and somatic sequelae of traumatic vaginal delivery: A literature review, Aust. N. Z. J. Obstet. Gynaecol. 55 (4) (2015) 309–314.

[6] E. Samuelsson, L. Ladfors, B. Lindblom, H. Hagberg, A prospective observational study on tears during vaginal delivery: Occurrences and risk factors, Acta Obs. Gynecol. Scand. 81 (1) (2002) 44–49.

[7] L.M. Hopkins, A.B. Caughey, D.V. Glidden, R.K. Laros Jr., Racial/ethnic differences in perineal, vaginal and cervical lacerations, Am. J. Obstet. Gynecol. 193 (2) (2005) 455–459.

[8] R.V. Krstic, Human Microscopic Anatomy: An Atlas for Students of Medicine and Biology, Springer Berlin Heidelberg, 1991.

[9] A. Huntington, K. Donaldson, R. De Vita, Contractile properties of vaginal tissue, J. Biomech. Eng. 142 (8) (2020) 080801.

[10] J. Dubik, M. Alperin, R. De Vita, The biomechanics of the vagina: A complete review of incomplete data, npj Women's Health 3 (1) (2025) 4.

[11] M. Farage, H. Maibach, Lifetime changes in the vulva and vagina, Arch. Gynecol. Obstet. 273 (4) (2006) 195–202.

[12] M.R. Routzong, G. Rostaminia, P.A. Moalli, S.D. Abramowitch, Pelvic floor shape variations during pregnancy and after vaginal delivery, Comput. Methods Programs Biomed. 194 (2020) 105516.

[13] J.M. McCracken, G.A. Calderon, A.J. Robinson, C.N. Sullivan, E. Cosgriff-Hernandez, J.C.E. Hakim, Animal models and alternatives in vaginal research: A comparative review, Reprod. Sci. 28 (2021) 1759–1773.

[14] A.C. Suarez, C.J. Gimenez, S.R. Russell, M. Wang, J.M. Munson, K.M. Myers, K.S. Miller, S.D. Abramowitch, R. De Vita, Pregnancy-induced remodeling of the murine reproductive tract: A longitudinal in vivo magnetic resonance imaging study, Sci. Rep. 14 (1) (2024) 586.

[15] D. Ulrich, S.L. Edwards, K. Su, J.F. White, J.A.M. Ramshaw, G. Jenkin, J. Deprest, A. Rosamilia, J.A. Werkmeister, C.E. Gargett, Influence of reproductive status on tissue composition and biomechanical properties of ovine vagina, PLoS One 9 (4) (2014) e93172.

[16] R. Rynkevic, P. Martins, L. Hympanova, H. Almeida, A.A. Fernandes, J. Deprest, Biomechanical and morphological properties of the multiparous ovine vagina and effect of subsequent pregnancy, J. Biomech. 57 (2017) 94–102.

[17] J.A. Daucher, K.A. Clark, D.B. Stolz, L.A. Meyn, P.A. Moalli, Adaptations of the rat vagina in pregnancy to accommodate delivery, Obs. Gynecol. 109 (1) (2007) 128–135.

[18] D.D. Rahn, M.D. Ruff, S.A. Brown, H.F. Tibbals, R.A. Word, Biomechanical properties of the vaginal wall: Effect of pregnancy, elastic fiber deficiency, and pelvic organ prolapse, Am. J. Obstet. Gynecol. 198 (5) (2008) 590–e1.

[19] J. Hamner, M. Florian-Rodriguez, J. Acevedo, H. Shi, R.A. Word, Protease inhibition improves healing of the vaginal wall after obstetrical injury: Results from a preclinical animal model, Sci. Rep. 10 (1) (2020) 6358.

[20] M. Alperin, A. Feola, R. Duerr, P. Moalli, S. Abramowitch, Pregnancy-and delivery-induced biomechanical changes in rat vagina persist postpartum, Int. Urogynecology J. 21 (2010) 1169–1174.

[21] C.A. Logan, L. Thiel, R. Bornemann, W. Koenig, F. Reister, H. Brenner, D. Rothenbacher, J. Genuneit, Delivery mode, duration of labor, and cord blood adiponectin, leptin, and C-reactive protein: Results of the population-based Ulm birth cohort studies, PLoS One 11 (2) (2016) e0149918.

[22] World Health Organization, WHO Recommendations on Intrapartum Care for a Positive Childbirth Experience, World Health Organization, 2018.

[23] M.J. Grimm, Forces involved with labor and delivery—A biomechanical perspective, Ann. Biomed. Eng. 49 (8) (2021) 1819–1835.

[24] E. Peña, B. Calvo, M.A. Martínez, P. Martins, T. Mascarenhas, R.M.N. Jorge, A. Ferreira, M. Doblaré, Experimental study and constitutive modeling of the viscoelastic mechanical properties of the human prolapsed vaginal tissue, Biomech. Model. Mechanobiol. 9 (1) (2010) 35–44.

[25] E. Pack, J. Dubik, W. Snyder, A. Simon, S. Clark, R. De Vita, Biaxial stress relaxation of vaginal tissue in pubertal gilts, J. Biomech. Eng. 142 (3) (2020) 031002.

[26] G.L. Clark-Patterson, J.A. McGuire, L. Desrosiers, L.R. Knoepp, R. De Vita, K.S. Miller, Investigation of murine vaginal creep response to altered mechanical loads, J. Biomech. Eng. 143 (12) (2021) 121008.

[27] J. Dubik, A. Tartaglione, K.S. Miller, D.A. Dillard, R. De Vita, History-dependent deformations of rat vaginas under inflation, Integr. Comp. Biol. 62 (3) (2022) 625–640.

[28] X. Fu, H. Siltberg, P. Johnson, U. Ulmsten, Viscoelastic properties and muscular function of the human anterior vaginal wall, Int. Urogynecology J. 6 (4) (1995) 229–234.

[29] G.L. Clark-Patterson, L.M. Buchanan, B.O. Ogola, M. Florian-Rodriguez, S.H. Lindsey, R. De Vita, K.S. Miller, Smooth muscle contribution to vaginal viscoelastic response, J. Mech. Behav. Biomed. Mater. 140 (2023) 105702.

[30] H.K. Weli, R. Akhtar, Z. Chang, W. Li, J. Cooper, Y. Yang, Advanced glycation products' levels and mechanical properties of vaginal tissue in pregnancy, Eur. J. Obs. Gynecol. Reprod. Biol. 214 (2017) 78–85.

[31] A. Feola, P. Moalli, M. Alperin, R. Duerr, R.E. Gandley, S. Abramowitch, Impact of pregnancy and vaginal delivery on the passive and active mechanics of the rat vagina, Ann. Biomed. Eng. 39 (2011) 549–558.

[32] J.L. Lowder, K.M. Debes, D.K. Moon, N. Howden, S.D. Abramowitch, P.A. Moalli, Biomechanical adaptations of the rat vagina and supportive tissues in pregnancy to accommodate delivery, Obs. Gynecol. 109 (1) (2007) 136–143.

[33] A.C. Suarez, K.S. Miller, K.M. Myers, S.D. Abramowitch, R. De Vita, Mechanical characterization of the murine reproductive tract through pregnancy and early postpartum recovery, Internat. J. Engrg. Sci. 226 (2026) 104579.

[34] S.L. Byers, M.V. Wiles, S.L. Dunn, R.A. Taft, Mouse estrous cycle identification tool and images, PloS One 7 (4) (2012) e35538.

[35] C.L. Lendon, M.J. Davies, G.V.R. Born, P.D. Richardson, Atherosclerotic plaque caps are locally weakened when macrophages density is increased, Atherosclerosis 87 (1) (1991) 87–90.

[36] G.A. Holzapfel, G. Sommer, P. Regitnig, Anisotropic mechanical properties of tissue components in human atherosclerotic plaques, J. Biomech. Eng. 126 (5) (2004) 657–665.

[37] J.A. McGuire, C.L. Crandall, S.D. Abramowitch, R. De Vita, Inflation and rupture of vaginal tissue, Interface Focus 9 (4) (2019) 20190029.

[38] G. Lionello, L. Cristofolini, A practical approach to optimizing the preparation of speckle patterns for digital-image correlation, Meas. Sci. Technol. 25 (10) (2014) 107001.

[39] S. Turner, Creep in glassy polymers, in: The Physics of Glassy Polymers, Springer, 1973, pp. 223–278.

[40] P.P. Provenzano, R.S. Lakes, D.T. Corr, R. Vanderby, Application of nonlinear viscoelastic models to describe ligament behavior, Biomech. Model. Mechanobiol. 1 (1) (2002) 45.

[41] J.A. McGuire, J.L. Monclova, A.C.S. Coariti, C.A. Stine, K.C. Toussaint Jr., J.M. Munson, D.A. Dillard, R. De Vita, Tear propagation in vaginal tissue under inflation, Acta Biomater. 127 (2021) 193–204.

[42] A.J. Huntington, B. Udayasuryan, P. Du, S.S. Verbridge, S.D. Abramowitch, R. De Vita, Smooth muscle organization and nerves in the rat vagina: A first look using tissue clearing and immunolabeling, Ann. Biomed. Eng. 50 (4) (2022) 440–451.

[43] P.A.L.S. Martins, E. Peña, B. Calvo, M. Doblaré, T. Mascarenhas, R. Natal Jorge, A. Ferreira, Prediction of nonlinear elastic behaviour of vaginal tissue: Experimental results and model formulation, Comput. Methods Biomech. Biomed. Eng. 13 (3) (2010) 327–337.

[44] R.D. Harkness, M.A. Nightingale, The extensibility of the cervix uteri of the rat at different times of pregnancy, J. Physiol. 160 (2) (1962) 214.

[45] K. Yoshida, M. Mahendroo, J. Vink, R. Wapner, K. Myers, Material properties of mouse cervical tissue in normal gestation, Acta Biomater. 36 (2016) 195–209.

[46] S. Nallasamy, K. Yoshida, M. Atkins, K. Myers, R. Iozzo, M. Mahendroo, Steroid hormones are key modulators of tissue mechanical function via regulation of collagen and elastic fibers, Endocrinology 158 (4) (2017) 950–962.

[47] C. Jayyosi, N. Lee, A. Willcockson, S. Nallasamy, M. Mahendroo, K. Myers, The mechanical response of the mouse cervix to tensile cyclic loading in term and preterm pregnancy, Acta Biomater. 78 (2018) 308–319.

[48] J. Vink, H. Feltovich, Cervical etiology of spontaneous preterm birth, in: Seminars in Fetal and Neonatal Medicine, Vol. 21, Elsevier, 2016, pp. 106–112.

[49] L.M. Silver, Mouse Genetics Concepts and Applications, Oxford University Press, 1995.

[50] C.P. Read, R.A. Word, M.A. Ruscheinsky, B.C. Timmons, M.S. Mahendroo, Cervical remodeling during pregnancy and parturition: Molecular characterization of the softening phase in mice, Reproduction 134 (2) (2007) 327–340.

[51] K. Genovese, Y.U. Lee, A.Y. Lee, J.D. Humphrey, An improved panoramic digital image correlation method for vascular strain analysis and material characterization, J. Mech. Behav. Biomed. Mater. 27 (2013) 132–142.

[52] P. Martins, A. Lopes Silva-Filho, A.M. Rodrigues Maciel da Fonseca, A. Santos, L. Santos, T. Mascarenhas, R.M. Natal Jorge, A.J.M. Ferreira, Biomechanical properties of vaginal tissue in women with pelvic organ prolapse, Gynecol. Obstet. Invest. 75 (2) (2013) 85–92.

[53] D. Ulrich, S.L. Edwards, V. Letouzey, K. Su, J.F. White, A. Rosamilia, C.E. Gargett, J.A. Werkmeister, Regional variation in tissue composition and biomechanical properties of postmenopausal ovine and human vagina, PLoS One 9 (8) (2014) e104972.

[54] J. Collins, Global epidemiology of multiple birth, Reprod. Biomed. Online 15 (2007) 45–52.

[55] J. Tuomi, Mammalian reproductive strategies: A generalized relation of litter size to body size, Oecologia 45 (1980) 39–44.

[56] S. Mesiano, T. Welsh, Progesterone and the control of human pregnancy and parturition, Fetal Matern. Med. Rev. 20 (2) (2009) 97–118.

[57] C.K. Ratajczak, J.C. Fay, L.J. Muglia, Preventing preterm birth: The past limitations and new potential of animal models, Dis. Model. Mech. 3 (7–8) (2010) 407–414.

[58] B. Fischer, P. Mitteroecker, Covariation between human pelvis shape, stature, and head size alleviates the obstetric dilemma, Proc. Natl. Acad. Sci. 112 (18) (2015) 5655–5660.

[59] B. Yang, P. Lee, Y. Hua, B. Brazile, S. Waxman, F. Ji, Z. Zhu, I.A. Sigal, Instant polarized light microscopy for imaging collagen microarchitecture and dynamics, J. Biophotonics 14 (2) (2021) e202000326.

[60] J. Dubik, A. Tartaglione, A. Wineman, D. Dillard, R. De Vita, A finite strain integral model for the creep behavior of vaginal tissue, Int. J. Non-Linear Mech. 162 (2024) 104729.

[61] W. Snyder, J.A. McGuire, C. Mou, D.A. Dillard, T. Iliescu, R. De Vita, Data-driven variational multiscale reduced order modeling of vaginal tissue inflation, Int. J. Numer. Methods Biomed. Eng. 39 (1) (2023) e3660.
[62] W. Snyder, A.S. Anaya, J. Krometis, T. Iliescu, R. De Vita, A numerical comparison of simplified galerkin and machine learning reduced order models for vaginal deformations, Comput. Math. Appl. 152 (2023) 168–180.
[63] A. Huntington, E. Rizzuto, S. Abramowitch, Z. Del Prete, R. De Vita, Anisotropy of the passive and active rat vagina under biaxial loading, Ann. Biomed. Eng. 47 (1) (2019) 272–281.
[64] A. Huntington, S.D. Abramowitch, P.A. Moalli, R. De Vita, Strains induced in the vagina by smooth muscle contractions, Acta Biomater. 129 (2021) 178–187.